2025 IEEE International Workshop on Metrology for AeroSpace, 18 - 20 Jun 2025, Naples, Italy

Calibration Accuracy of RCS Measurements in Free Space

P. D. Thusitha Wickramasinghe
Centre for Defence Engineering and Physical Science
Cranfield University
Defence Academy of the UK
Shrivenham, SN6 8LA
t.wickramasinghe@cranfield.ac.uk

Alessio Balleri
Centre for Defence Engineering and Physical Science
Cranfield University
Defence Academy of the UK
Shrivenham, SN6 8LA
a.balleri@cranfield.ac.uk

***Abstract*—When investigating Radar Cross Section (RCS) of targets, it is essential to establish confidence in the experimental calibration data. In this paper, experiments are presented which were carried out to determine the calibration accuracy achieved in performing free space target RCS measurements in the radar lab at Cranfield University. Calibration data were collected in the X-band (between 8.5 GHz and 12 GHz) using four off-the-shelf non-calibrated metallic spheres of different diameter: 30 mm, 38 mm, 80 mm and 100 mm. The results indicate an accuracy of less than ± 2 dBm^2 for the spheres measured on a styrofoam stand and with a Signal to Noise Ratio (SNR) of at least 40 dB for all spheres.**

***Index Terms*—Radar Cross Section, RCS Calibration**

I. Introduction

Measuring the radar reflective properties of targets by characterising their target RCS is a very important task to aid the design and development of radar systems and relative countermeasures. To accurately measure the RCS of a target, the associated calibration errors should be minimal [1] [2].

In our previous work, we have measured and analysed the RCS of various targets, with particular attention to drones [3] [4] [5]. However, the radar lab at Cranfield university does not feature an anechoic chamber and the calibrating targets typically used are standard low-cost off-the-shelf metallic spheres (or other uncalibrated reference objects). Because of this, errors are normally expected to occur due to non-resolvable multi-path interference between the target under test and the support structures as well as due to non-perfect (non-calibrated) calibrating targets.

In this paper, the objective of investigating RCS measurement errors is achieved by experimenting with four off-the-shelf metallic spheres with different sizes in several experimental configurations. The spheres are chosen due to the ease in estimating their theoretical RCS and because their theoretical RCS does not depend on aspect angle.

II. Experimental Setup

An MS46322A Anritsu Vector Network Analyser (VNA) was used to collect data between 8.5 GHz and 12 GHz with 4001 frequency samples spaced at 1 MHz. The VNA was connected to two standard 5.5x4 cm horn antennas, which were used to transmit and receive signals in VV-polarisation, and to a PC with an ethernet cable so that measurements could be fully controlled with LabView.

To analyse the calibration accuracy, four off-the-shelf metallic spheres were measured at a distance of approximately 2 m from the antennas. The far-field (i.e. Fraunhofer region) was calculated to be at 0.833m [6] but a longer distance was chosen to isolate the sphere returns from strong antenna coupling and, simultaneously, reduce multipath contributions. Some Radar Absorbent Material (RAM) was positioned around the setup to mitigate the effects of unwanted reflections from the surrounding open laboratory area. To ensure the spheres were aligned with the antenna in elevation, a laser alignment equipment was used to level the antenna and the spheres (see Fig. 1).

The analysis of accuracy was carried out on four distinct configurations with the spheres placed on a styrofoam stand as shown in Fig. 1: with the laboratory lights on and off, and with and without RAM behind the spheres. Comparisons between

Fig. 1. Experiments setup with the spehere on the styrofoam (left) and with the laser-level system (right).

the calibration accuracy for the spheres were carried out to investigate the quality of the calibrating targets, the impact of the interactions with the lights and the presence of the RAM on the calibration results. For each measurement of the spheres, a background measurement was taken and removed from the data to remove clutter contributions.

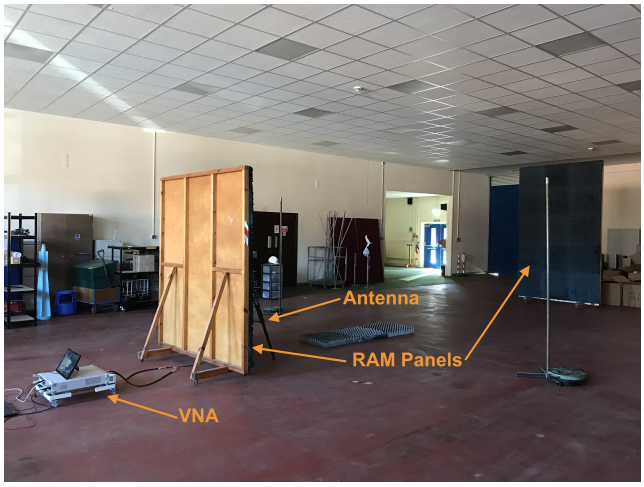

Fig. 2. Photo of the experimental setup with the VNA and the RAM panels.

The Fig. 2 shows a photo of the experimental setup, and the RAM panel behind the antennas remained in place for all measurements to prevent any signal reflection from the clutter behind the antennas.

III. Calibration Methodology

Initially, the VNA is calibrated so as to provide a flat frequency response when the transmit and receive channels are connected to each other with a through connector. The measurement setup is then modelled as a Linear Time Invariant (LTI) system so that for an input signal $x(t)$ the system response $y(t)$ is a function of the impulse response $h(t)$ as

$$y(t) = \int_{+\infty}^{-\infty} h(\tau) * x(t-\tau) d\tau \tag{1}$$

For an input signal $x(t) = e^{i2\pi f_0 t}$, the output can be expressed as

$$y(t) = e^{i2\pi f_0 t} \cdot H(f_0) \tag{2}$$

where $H(f_0)$ indicates the Fourier transform of $h(t)$ at the frequency f_0. The VNA sweeps all frequencies by transmitting a stepped-frequency signal to provide the values of $H(f_i)$ for all frequency points f_i. To eliminate multi-path contributions, the Inverse Fast Fourier Transform (IFFT) of $H(f_i)$ is applied to isolate in range the components of the response of the target of interest. This is obtained with the use of a window applied to the time domain signal resulting from the IFFT. The amplitude squared of the FFT of the range-limited signal $\hat{H}(f_i)$ is a scaled function of the received power P_r, which is a function of the target RCS σ as [7, pp. 100]

$$P_r = \frac{P_t G_t}{4\pi R^2} \times \frac{A_e}{4\pi R^2 L_T} \times \sigma \tag{3}$$

where P_t is the transmit power, G_t is the transmit antenna gain, R is the target range, A_e is the effective receive antenna area and L_T is the total signal loss. In (3), only the RCS σ is related to the target and the remaining variables are associated to external factors such as environmental, antenna etc. To obtain the target RCS a substitution technique [8] is used after observing that for two targets at the same range

$$\frac{P_r^1}{P_r^2} = \frac{\sigma_1}{\sigma_2} = \frac{|\hat{H}_1(f_i)|^2}{|\hat{H}_2(f_i)|^2} \tag{4}$$

where the dependency of the received power and target RCS on the frequency f_i has been omitted for simplicity. As there are 4 spheres, each sphere at a time was used as the calibrating target. A calibration vector for each calibrating sphere was obtained as the dB difference between the theoretical RCS and the power of the measured signature. The obtained calibrating vector is then applied to the measurements of the remaining three spheres to obtain their calibrated RCS. This method was repeated when all three spheres were used as the calibrating target. Given the sphere sizes and the measurement frequency band, the theoretical RCS was calculated using the sphere RCS equations valid for the Mie region [9].

IV. Results

The results shown in Fig. 3 to Fig. 14 show the calibration error for any combination, i.e. the difference between the theoretical and the calibrated RCS signatures of a given sphere against each other obtained with the procedure presented in Section III. In the figures, 'wRAM' indicates the experiments were conducted with the RAM behind the targets, whilst 'nRAM' indicates the experiments were conducted without it. Similarly, 'wLight' indicates results obtained with the ceiling lights turned on and 'nLight' with the lights turned off. For all spheres, the range limited time signals showed a SNR of at least 40 dB.

Results show the errors remain within ± 2 dBm^2 for all possible combinations. They also show that errors are very similar in all four experimental configurations, indicating that the presence of the RAM at the back of the targets and the laboratory lights did not have a large impact at these frequencies.

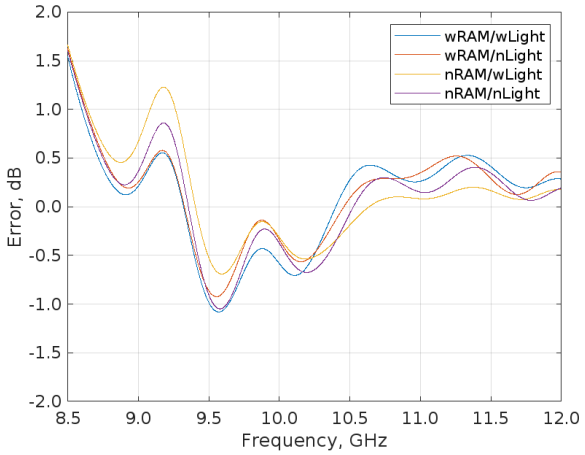

Fig. 3. Calibration error in dBm^2 of the 30 mm sphere calibrated against the 38 mm sphere.

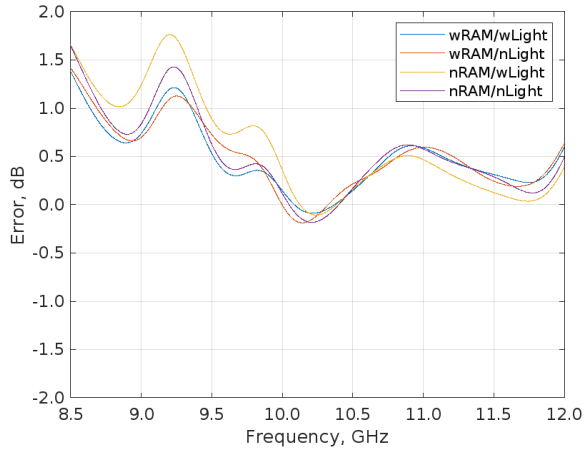

Fig. 4. Calibration error in dBm^2 of the 30 mm sphere calibrated against the 80 mm sphere.

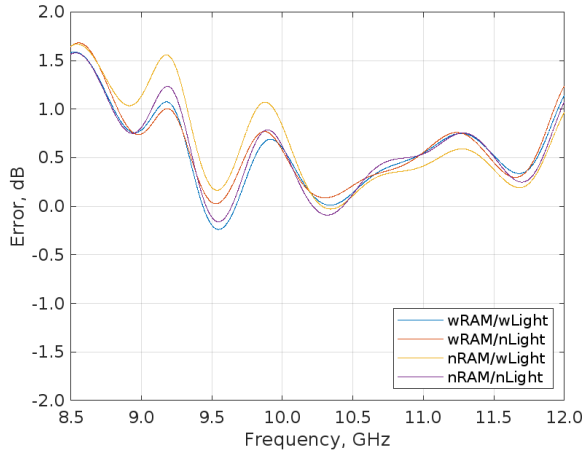

Fig. 5. Calibration error in dBm^2 of the 30 mm sphere calibrated against the 100 mm sphere.

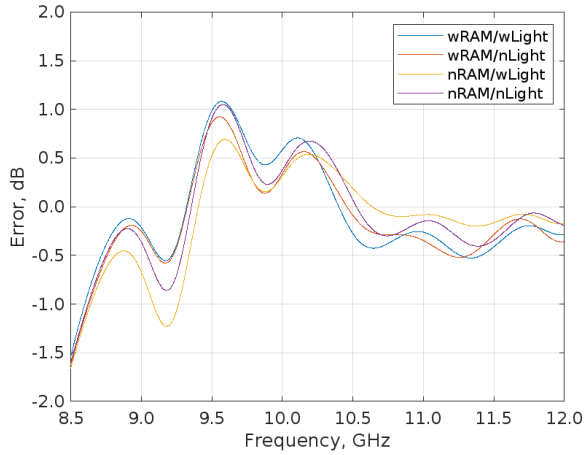

Fig. 6. Calibration error in dBm^2 of the 38 mm sphere calibrated against the 30 mm sphere.

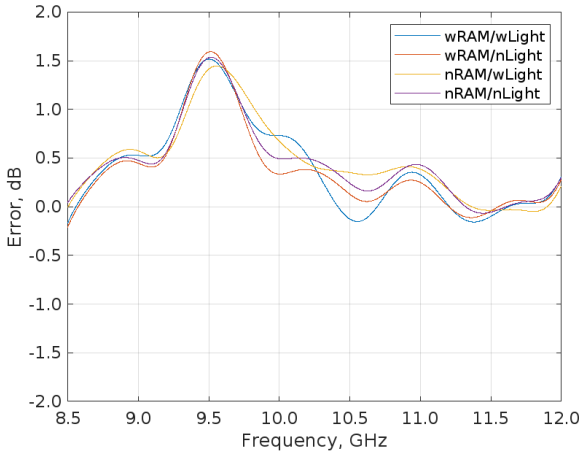

Fig. 7. Calibration error in dBm^2 of the 38 mm sphere calibrated against the 80 mm sphere.

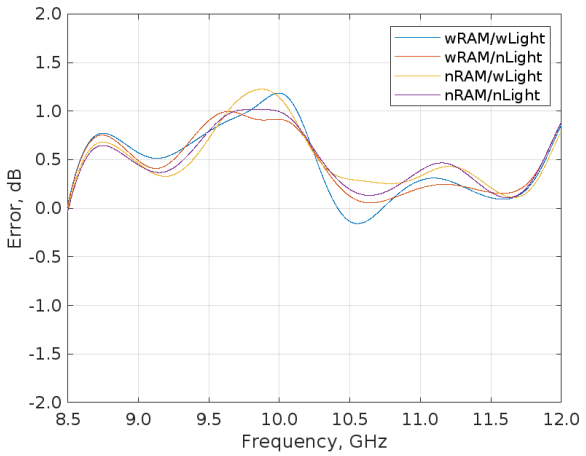

Fig. 8. Calibration error in dBm^2 of the 38 mm sphere calibrated against the 100 mm sphere.

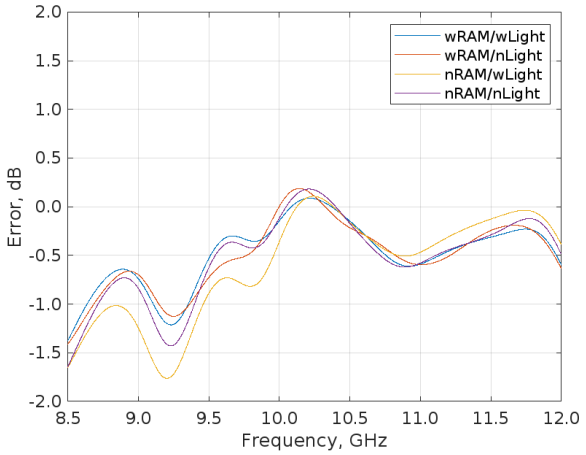

Fig. 9. Calibration error in dBm^2 of the 80 mm sphere calibrated against the 30 mm sphere.

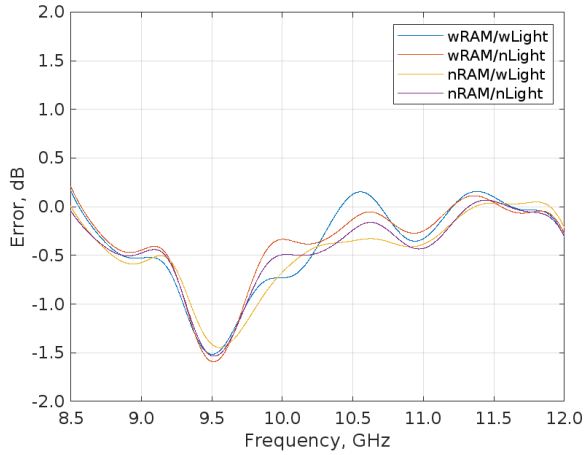

Fig. 10. Calibration error in dBm^2 of the 80 mm sphere calibrated against the 38 mm sphere.

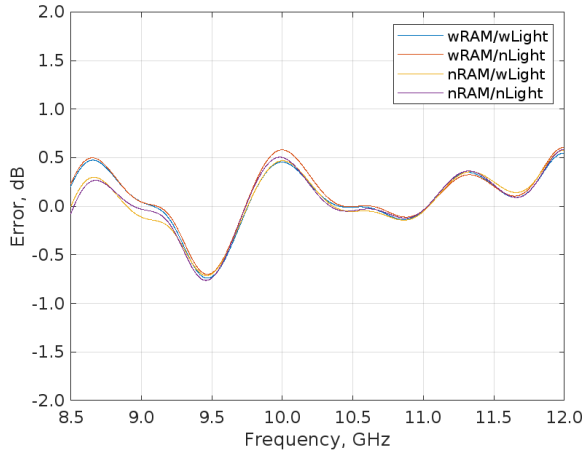

Fig. 11. Calibration error in dBm^2 of the 80 mm sphere calibrated against the 100 mm sphere.

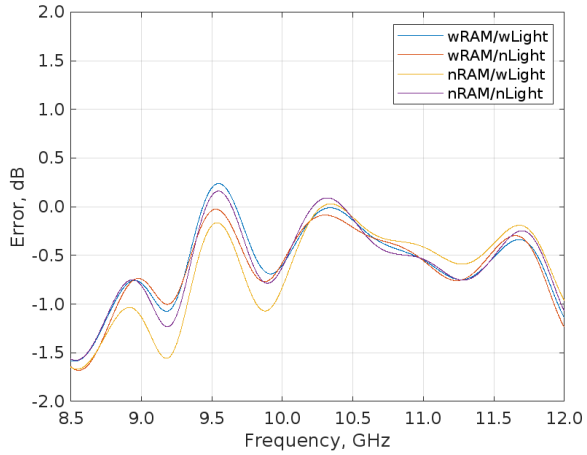

Fig. 12. Calibration error in dBm^2 of the 100 mm sphere calibrated against the 30 mm sphere.

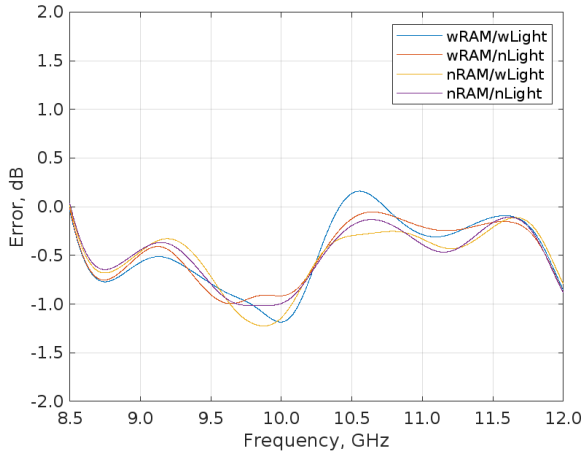

Fig. 13. Calibration error in dBm^2 of the 100 mm sphere calibrated against the 38 mm sphere.

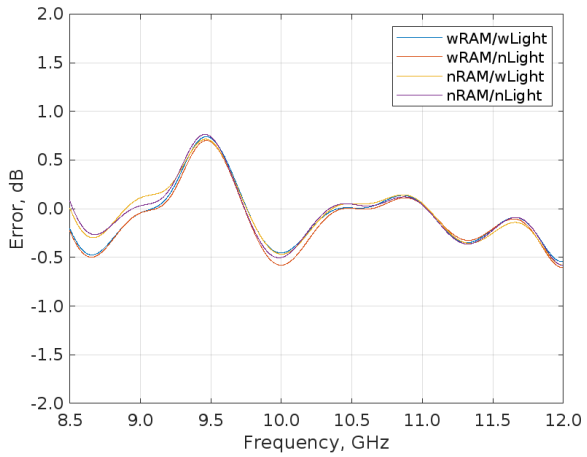

Fig. 14. Calibration error in dBm^2 of 100 mm sphere calibrated against 80 mm sphere.

The results in Fig. 15 to Fig. 22 show the statistics of the calibration errors presented in Fig. 3 to Fig. 14. In the figures, the shape of the marker represents a particular sphere size, while the colour represents the following experimental setup configuration:

- wRAM / wLight : Blue
- wRAM / nLight : Purple
- nRAM / wLight : Green
- nRAM / nLight : Yellow

The description of each configuration presented above (i.e. wRAM, wLight etc.) is the same as previously described.

Results show that overall the the mean error is consistent between all calibrating spheres with values oscillating either around 0.6 dBm^2 or -0.6 dBm^2. The smallest maximum errors are obtained when the spheres are calibrated against the 38 mm sphere but, otherwise, the maximum and minimum errors assume values just below 1.8 dBm^2 for all other combinations.

A summary of the experimental results is provided in Table I which indicates the minimum and maximum mean value, standard deviation (STD) and error between all the measurements. In the table, Exp/Cal is used to indicated to the experimented sphere and the calibrating sphere. The table corroborates that the maximum and minimum error found between all measurements is below 2 dBm^2.

TABLE I
STATISTICAL RESULT SUMMARY

	Min		Max	
Stat.	**Value**	**Exp/Cal**	**Value**	**Exp/Cal**
Mean	-0.69	100/30	0.69	30/100
STD	0.29	80/100	0.50	80/30
Error	-1.76	80/30	1.76	30/80

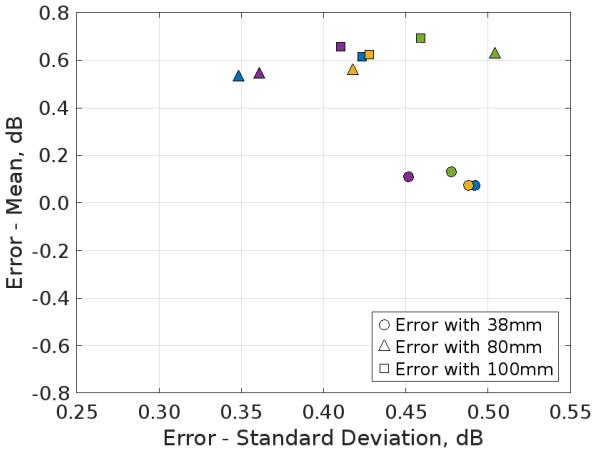

Fig. 15. Mean/Std. error statistics of calibrated 30 mm sphere.

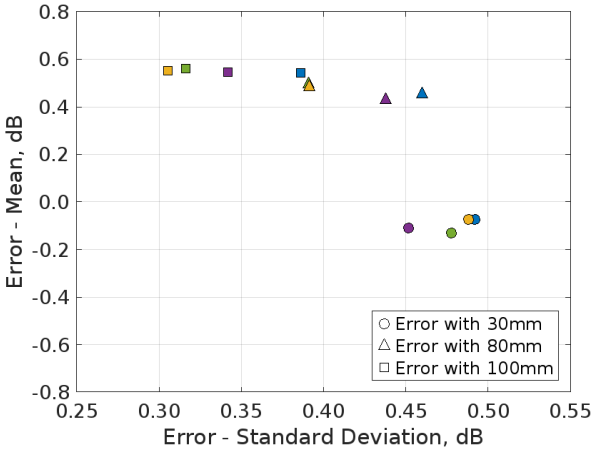

Fig. 16. Mean/Std. error statistics of calibrated 38 mm sphere.

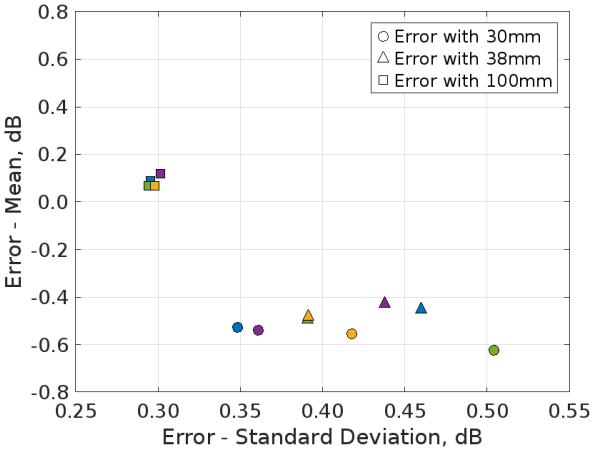

Fig. 17. Mean/Std. error statistics of calibrated 80 mm sphere.

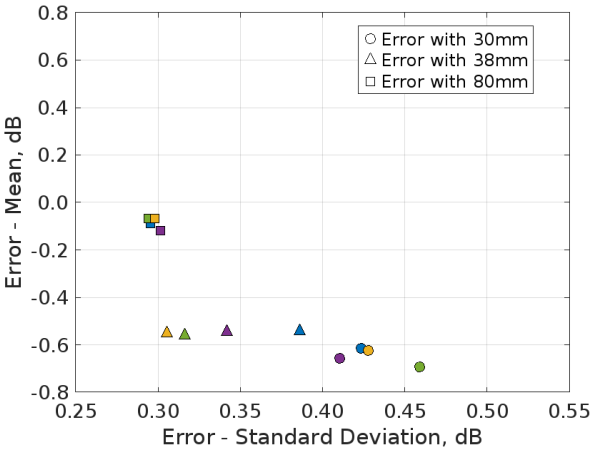

Fig. 18. Mean/Std. error statistics of calibrated 100 mm sphere.

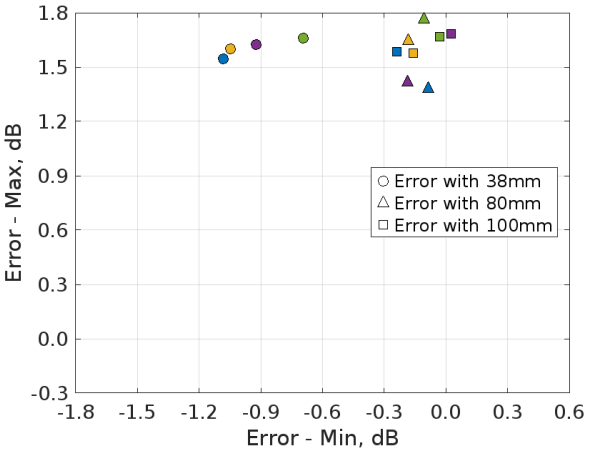

Fig. 19. Min/Max error statistics of calibrated 30 mm sphere.

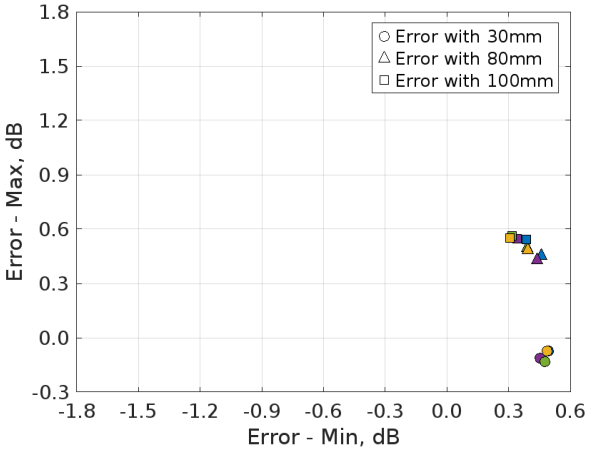

Fig. 20. Min/Max error statistics of calibrated 38 mm sphere.

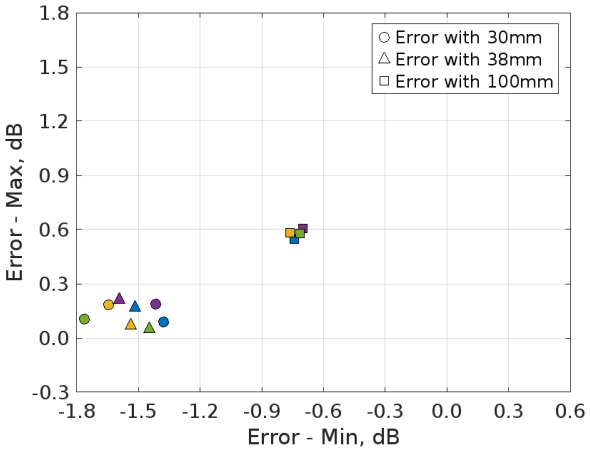

Fig. 21. Min/Max error statistics of calibrated 80 mm sphere.

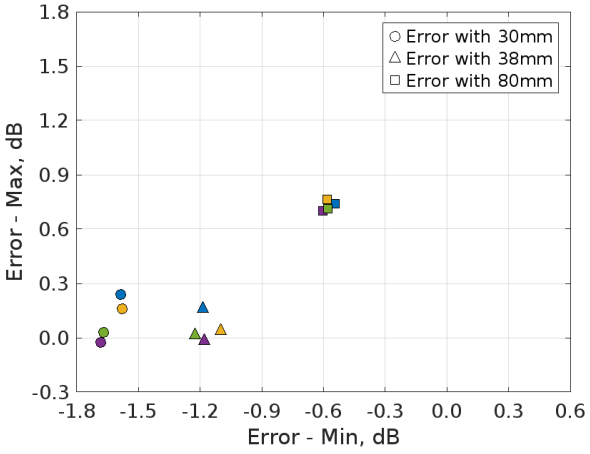

Fig. 22. Min/Max error statistics of calibrated 100 mm sphere.

V. Conclusions

This paper presents measurements to characterise the calibration accuracy of RCS measurements. Data was collected in the X-band, from 8.5 GHz to 12 GHz, for four off-the-shelf metallic spheres with 30 mm, 38 mm, 80 mm and 100 mm diameter. Data was taken in various configurations to assess the impact of laboratory lights and RAM material on the results.

Results have shown the accuracy remains within ± 2 dBm^2 and that differences to changes in the setup configurations were minor at these frequencies.

An additional setup with spheres suspended on a string to eliminate interactions with the stand was also investigated. However, the results with this setup were significantly compromised because it remained impossible to measure completely static spheres.

Data Availability Statement

Data supporting this study cannot be made available due to commercial restrictions.

References

[1] B. Kent, "Comparative measurements of precision radar cross section (rcs) calibration targets," in *IEEE Antennas and Propagation Society International Symposium. 2001 Digest. Held in conjunction with: USNC/URSI National Radio Science Meeting (Cat. No.01CH37229)*, vol. 4, 2001, pp. 412–415 vol.4.

[2] R. E. Jarvis, J. G. Metcalf, J. E. Ruyle, and J. W. McDaniel, "Wideband measurement techniques for extracting accurate rcs of single and distributed targets," *IEEE Transactions on Instrumentation and Measurement*, vol. 71, pp. 1–12, 2022.

[3] M. Rosamilia, A. Aubry, A. Balleri, V. Carotenuto, and A. De Maio, "Rcs measurements of uavs and their statistical analysis," in *2022 IEEE 9th International Workshop on Metrology for AeroSpace (MetroAeroSpace)*, 2022, pp. 179–184.

[4] ——, "Radar detection performance via frequency agility using measured uavs rcs data," *IEEE Sensors Journal*, vol. 23, no. 19, pp. 23 011–23 019, 2023.

[5] M. Rosamilia, A. Balleri, A. De Maio, A. Aubry, and V. Carotenuto, "Radar detection performance prediction using measured uavs rcs data," *IEEE Transactions on Aerospace and Electronic Systems*, vol. 59, no. 4, pp. 3550–3565, 2023.

[6] A. Capozzoli, C. Curcio, F. D'Agostino, and A. Liseno, "A review of the antenna field regions," *Electronics*, vol. 13, no. 11, 2024. [Online]. Available: https://www.mdpi.com/2079-9292/13/11/2194

[7] M. Skonik, *Radar Handbook*, 3rd ed. McGraw Hill, 2008.

[8] E. Walton *et al.*, "Ieee recommended practice for radar cross-section test procedures," *IEEE Press*, 2007.

[9] B. R. Mahafza, *Radar systems analysis and design using MATLAB*. Chapman and Hall/CRC, 2005.

Calibration accuracy of RCS measurements in free space

Wickramasinghe, Pathiraja

2025-06-20

Wickramasinghe P, Balleri A. (2025) Calibration accuracy of RCS measurements in free space.
In: 2025 IEEE International Workshop on Metrology for AeroSpace, 18 - 20 Jun 2025, Naples, Italy
https://doi.org/10.1109/MetroAeroSpace64938.2025.11114705